Applied Physics Express

The Japan Society of Applied Physics

LETTERS

High-efficiency electron-beam-pumped sub-240-nm ultraviolet emitters based on ultra-thin GaN/AlN multiple quantum wells grown by plasma-assisted molecular-beam epitaxy on *c*-Al_2O_3

To cite this article: Valentin N. Jmerik *et al* 2018 *Appl. Phys. Express* **11** 091003

View the article online for updates and enhancements.

You may also like

- Deep-ultraviolet integrated photonic and optoelectronic devices: A prospect of the hybridization of group III–nitrides, III–oxides, and two-dimensional materials
Nasir Alfaraj, Jung-Wook Min, Chun Hong Kang et al.
- III-nitride semiconductors for intersubband optoelectronics: a review
M Beeler, E Trichas and E Monroy
- Assessment of AlGaN/AlN superlattices on GaN nanowires as active region of electron-pumped ultraviolet sources
I Dimkou, A Harikumar, F Donatini et al.

This content was downloaded from IP address 18.119.107.96 on 25/04/2024 at 03:00

Applied Physics Express **11**, 091003 (2018)
https://doi.org/**10.7567/APEX.11.091003**

High-efficiency electron-beam-pumped sub-240-nm ultraviolet emitters based on ultra-thin GaN/AlN multiple quantum wells grown by plasma-assisted molecular-beam epitaxy on *c*-Al_2O_3

Valentin N. Jmerik[1*], Dmitrii V. Nechaev[1], Alexey A. Toropov[1], Evgenii A. Evropeitsev[1], Vladimir I. Kozlovsky[2], Victor P. Martovitsky[2], Sergey Rouvimov[1,3], and Sergey V. Ivanov[1]

[1]*Ioffe Institute, St. Petersburg 194021, Russia*
[2]*Lebedev Physical Institute, Moscow 119991, Russia*
[3]*University of Notre Dame, Notre Dame, IN 46556, U.S.A.*

*E-mail: jmerik@pls.ioffe.ru

Received June 1, 2018; accepted July 27, 2018; published online August 22, 2018

We report the internal structures and emission properties of GaN/AlN single- and multiple-quantum-well (QW) heterostructures with well widths of $d_w = 1$–4 monolayers (MLs), grown by plasma-assisted molecular-beam epitaxy on *c*-sapphire at metal-rich conditions and low temperatures (~700 °C). The formation of plane QWs with abrupt symmetrical interfaces is confirmed by both scanning transmission electron microscopy and X-ray diffraction analysis. Pulse-scanning and continuous-wave output powers of 150 and 28 mW, respectively, at a peak emission wavelength of 235 nm were achieved at 300 K in an electron-beam-pumped deep-ultraviolet (1.5 ML-GaN/5.5 nm-AlN)$_{360}$ multiple-QW emitter with a maximum efficiency of 0.75%. © 2018 The Japan Society of Applied Physics

The wide-gap (Al,Ga)N compounds are basic semiconductor materials for ultraviolet (UV) photonic devices required for the germicidal optical treatment of water/air/surface at both standard wavelengths of 264 and 222 nm in the far UV-C range (for an in vivo treatment), as well as for optical spectroscopy, communication, etc.[1,2] Deep-UV light-emitters are currently based mainly on $Al_xGa_{1-x}N/Al_yGa_{1-y}N$ ($x = 0.4$–0.8, y–$x = 0.1$–0.4) quantum-well (QW) heterostructures with a typical well width of $d_w = 1$–2 nm.

However, several serious challenges exist in the fabrication of deep-UV-emitting devices based on wurtzite (Al,Ga)N QW heterostructures grown on *c*-sapphire substrates. First, a strong polarization field emerging in the QWs leads to the quantum-confined Stark effect (QCSE) with the strong electron–hole separation inside the QWs, which leads to both reduction in their internal quantum efficiency (IQE) and significant red-shift of the emission wavelength.[3] Second, the complex valence band structure of the AlGaN alloys undergoes a band crossover at $x \sim 25$ mol %, when the split-off sub-band becomes a topmost valence sub-band.[4] This leads to a transverse-magnetic-(TM)-polarized ($E \parallel c$-axis) inter-band emission, which has a significantly lower extraction efficiency through the basal plane, compared to the transverse-electric-(TE)-polarized UV light observed in low-Al-content alloys where the top position in the valence band is occupied by the heavy-hole sub-band.

In order to overcome these problems, deep-UV light emitters based on ternary $Al_xGa_{1-x}N/Al_yGa_{1-y}N$ ($x \ll y$) or binary GaN/AlN QW structures with d_w as small as ~1 monolayer (ML) were proposed theoretically[5] and studied experimentally.[6–8] Plasma-assisted molecular-beam epitaxy (PAMBE) performed at relatively low growth temperatures [$T_S = 700$–750 °C for (Al)GaN layers] and growth rates (below 0.5 ML/s) has large potential for development of the atomically resolved technology of the (Al,Ga)N QW heterostructures. We have already used these advantages of PAMBE to realize a sub-monolayer digital alloying (SDA) technique for growth of the $Al_xGa_{1-x}N/Al_yGa_{1-y}N$ QWs as nominal $\{GaN/Al_yGa_{1-y}N\}_N$ ($N = 2$–10) superlattices (SLs) with extremely thin (<1 ML) GaN insertions.[9] The high efficiency of radiative recombination in the SDA single-QW (SQW) structures has been confirmed by observation of stimulated emission in the λ range of 258–303 nm with a minimum threshold power density of ~150 kW/cm^2 ($\lambda = 290$ nm).[10] In addition, a high-intensity spontaneous UV-radiation at $\lambda = 285$ nm with an output power of $P_{out} = 160$ (39) mW, excited by an e-beam in a pulse-scanning [continuous wave (CW)] mode, respectively, has been demonstrated in AlGaN MQW heterostructures fabricated by the SDA technique.[11]

Extremely thin binary GaN/AlN multiple-QW (MQW) structures with d_w of few MLs were fabricated by both metal–organic vapor phase epitaxy (MOVPE)[12] and PAMBE.[13] Using PAMBE, Islam et al. have demonstrated a TE-polarized photoluminescence (PL) at the shortest wavelength of 219 nm.[14] They used either standard or modified Stranski–Krastanov growth modes under N-rich conditions ($F_{Ga}/F_N < 1$) to induce formation of three-dimensional (3D) GaN islands (dots/disks) into GaN QWs with nominal thicknesses of 1–3 MLs. Despite the enhanced PL IQE and TE-polarization of the output emission, the maximum achieved output power density of the GaN/AlN QW UV-light-emitting diodes (LEDs) at the shortest $\lambda = 234$ nm was below 0.4 mW/cm^2.[15]

Additional factors contributing to the low values of the efficiency and output power of such sub-250-nm UV-LEDs are the poor p-type conductivity of $Al_xGa_{1-x}N$ layers with $x = 0.4$–1 and high resistance of their ohmic contacts.[16] The importance of these problems can be illustrated by the observation that UV-LEDs with a standard AlGaN-based QW design, grown on bulk AlN substrates, exhibit the highest output CW power of 150 mW only for wavelengths longer than 265 nm.[17] However, UV-LEDs emitting at a shorter wavelength (226 nm) have the maximum output power of only 225 μW even in the case of specially designed diode structures grown on bulk AlN substrates, which is primarily associated with an insufficient p-doping of AlGaN layers with a high Al content used in these diodes.[18] These problems can be avoided in e-beam-pumped (EBP) UV-emitters, which, in addition, can be designed with a thick MQW active region to yield a higher output power. Several groups have developed such type of deep-UV light sources[11,19–22] with a maximum $P_{out} \sim 230$ mW at $\lambda =$

 © 2018 The Japan Society of Applied Physics

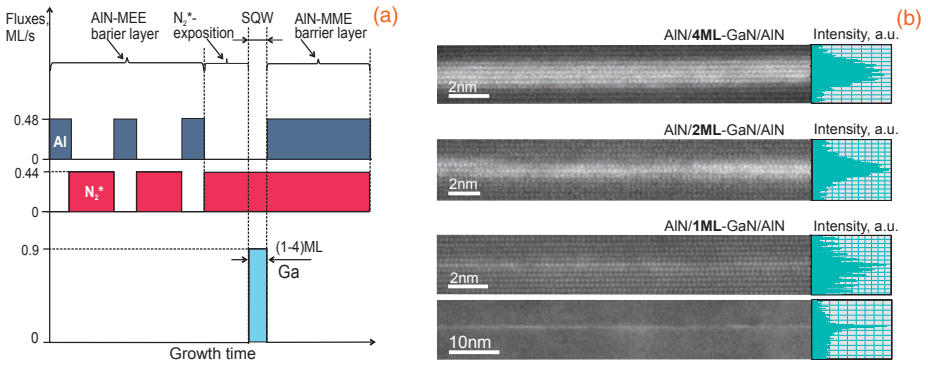

Fig. 1. (a) Typical shutter sequence during the growth of a GaN/AlN QW. (b) HAADF-STEM images of GaN/AlN SQW structures with nominal thicknesses varied from 1 to 4 MLs. An integrated distribution of the STEM image brightness is plotted on the right side of each image.

246 nm using an e-beam energy of $E = 12$ keV and pulsed current of $I_e = 4.4$ mA for excitation.[23)]

In this study, we report a PAMBE growth as well as structural and optical properties of GaN/AlN SQW and MQW structures, with nominal thicknesses of the GaN QWs varied in the range of 1–4 MLs, grown at metal-rich conditions. The emission efficiency of a sub-240-nm UV radiation was probed to be 0.75% under e-beam excitation conditions in GaN/AlN MQW structures with a number of 1.5-ML-thick QWs as large as 360.

All of the samples were grown in a PAMBE setup Compact 21T (Riber) on standard annealed and nitridated c-Al_2O_3 substrates over 65-nm-thick two-dimensional (2D) AlN nucleation layers deposited by migration-enhanced epitaxy (MEE).[24)] AlN buffers with a thickness of ~1.5 μm were then grown by metal-modulated epitaxy (MME) under slightly Al-rich conditions and $T_S = 780$ °C.[25)] The $\{GaN/AlN\}_N$ ($N = 1$–360) MQW structures with GaN and AlN layer thicknesses varied in the ranges of 0.5–4 MLs and 5–40 nm, respectively, were grown at constant $T_S = 700$ °C and nitrogen flux of $F_N = 0.44$ ML/s. Me-rich conditions were used in the growth of both layers at flux ratios of $F_{Ga}/F_N \sim 2$ and $F_{Al}/F_N \sim 1.05$, which allowed us to control the nominal well and barrier thicknesses using the calibrated N flux. Figure 1(a) schematically illustrates the growth sequence of one period of the GaN/AlN MQW structures. In order to eliminate the excess metal from the Al-adlayer on the AlN barrier surface before the growth of the GaN QW, three MEE cycles of AlN growth followed by its surface exposure to a nitrogen flux were applied. The excessive Ga remaining on the QW growth surface was segregated automatically into a floating layer on the surface of the top AlN barrier, owing to the lower GaN binding energy than that of AlN, and evaporated at the employed T_S. This procedure ensured the fabrication of a 1–4-ML-thick GaN QW with symmetric abrupt interfaces [Fig. 1(b)].

The growth was monitored in situ by reflection high-energy electron diffraction (RHEED), laser reflection (LR), and home-made multi-beam optical stress sensor (MOSS) with a measurement frequency of 10 Hz. Ex situ studies of the structures were performed using high-angle annular dark-field scanning transmission electron microscopy (HAADF STEM; Titan 350) and X-ray diffraction (XRD) with a triple crystal geometry and Cu Kα radiation ($\lambda = 1.5406$ Å) monochromatized by a two-bounce Ge(220) crystal combined with a parabolic X-ray mirror and third 3× Ge(220) analyzer.

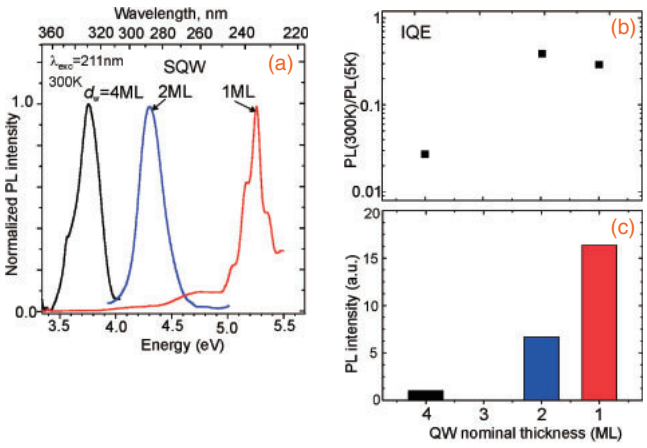

Fig. 2. (a) Normalized PL spectra measured at RT for GaN/AlN SQW structures with well widths varied in the range of $d_w = 1$–4 MLs, and (b) ratios of integrated PL intensities measured at RT and 5 K (IQE) and (c) relative integrated RT PL intensities as a function of the nominal well thickness.

PL spectra were measured at 5 and 300 K with excitation by a fourth-harmonic of a femtosecond Ti:sapphire laser at 211 nm. Cathodoluminescence (CL) spectra were measured through a substrate and quartz glass using pulse-scanning and CW modes of electron-beam excitation from the structure surface with spot diameters of 1 and 10 mm, respectively, energy of 10–20 kV, and beam current varied up to 1 mA, as described in previous studies.[11,22)]

Figure 1(b) shows Z-contrast HAADF-STEM images of GaN/AlN SQW structures with d_w varying from 1 to 4 MLs, which correspond to the nominal values with an accuracy of ~0.5 ML. All of the wells exhibit symmetric Ga distributions in the growth direction, thus indicating the absence of Ga segregation phenomena[26,27)] in the structures grown at $T_S = 700$ °C.

Some lateral inhomogeneities of Z-contrast along the GaN/AlN QWs, particularly pronounced in the thinnest QW, are observed and will be discussed below. The SQW structures exhibit single PL peaks up to room temperature (RT), as shown in Fig. 2(a). The PL peak positions shift from 330 to 235 nm with the decrease in d_w from 4 to 1 ML, which was previously described theoretically and observed experimentally for short-period GaN/AlN SLs with few-ML-thick GaN QWs grown by MOVPE[12)] or PAMBE.[13)] Surprisingly, the full-width-at-half-maximum (FWHM) values of the RT PL peaks do not exceed 8 nm (~ 0.2 eV) in the complete range

© 2018 The Japan Society of Applied Physics

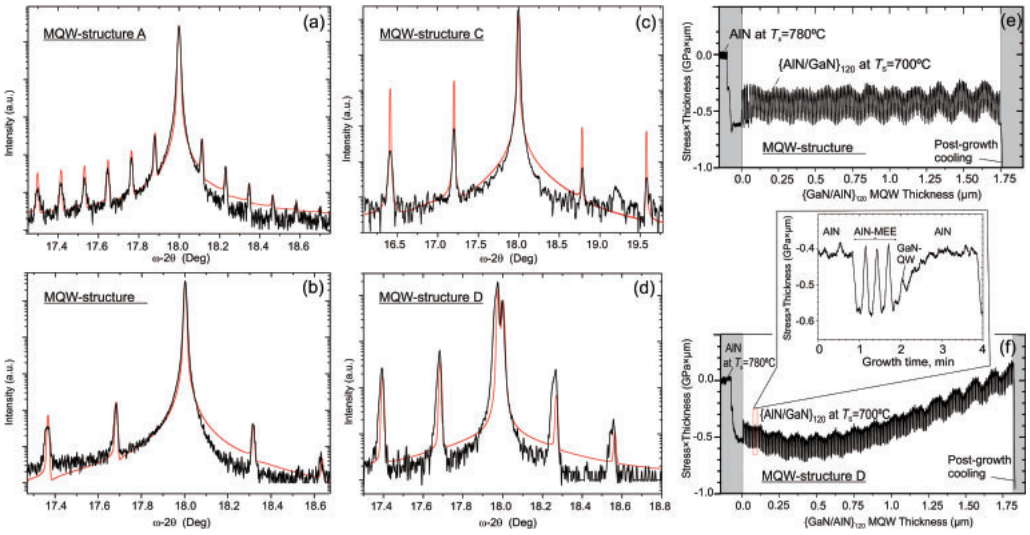

Fig. 3. HRXRD $\omega/2\theta$ scans of (0002) reflections of GaN/AlN MQW structures with varied numbers (N) of QWs and nominal QW (d_w) and barrier (D_{AlN}) thicknesses: (a) $d_w = 1.5$ ML, $D_{AlN} = 38.5$ nm, $N = 40$ (structure A), (b) $d_w = 1.5$ ML, $D_{AlN} = 15.5$ nm, $N = 120$ (structure B), (c) $d_w = 1.5$ ML, $D_{AlN} = 5.5$ nm, $N = 360$ (structure C), and (d) $d_w = 4$ MLs, $D_{AlN} = 15.5$ nm, $N = 120$ (structure D). The black curves are experimental curves, while the red are simulation curves. (e) and (f) Temporal evolutions of the substrate curvatures (stress×thickness) during the PAMBE growth runs of structures B and D, respectively. Inset in (f) shows the (stress×thickness) variation at high magnification during growth of a single QW.

of QW thicknesses. Moreover, an evaluation of the IQEs of the set of SQWs, based on measurements of the PL_{300K}/PL_{5K} ratios of integrated intensities, reveals a significantly higher IQE (up to 45%) in the 1–2-ML-thick QWs, which was reduced down to 3% when d_w reached 4 MLs. The latter is a typical value for GaN/AlN structures with $d_w > 1$ nm,[28] while the former exceeds the maximum value of 40% reported for similar GaN/AlN QWs grown by PAMBE at N-rich conditions.[13] The thinnest GaN/AlN QW structure also exhibits an order of magnitude higher RT integrated PL intensity compared to the thicker structures [Fig. 2(c)]. The PL peak positions of these structures (not shown) practically do not change with the increase in the temperature up to approximately 150 K and then undergo a red-shift by only 20 meV with the increase in the temperature to 300 K.

The observed variations in the SQW PL properties with the GaN thickness are related to the reduction in the spatial separation of electrons and holes by the polarization fields in the extremely thin GaN/AlN QWs (≤2 MLs). Other possible factors could be a contribution of lateral carrier confinement induced by the fluctuations of the QW width/composition, observed in the STEM images, and suppression of the valence band structure crossover[5] in the thin GaN QWs, which ensures TE polarization of the PL emission from these structures, observed experimentally.

Figure 3 shows high-resolution (HR) XRD $\omega/2\theta$ scans of the (0002) reflections of the GaN/AlN MQW structures with different numbers of GaN QWs as well as different well and period thicknesses. The figure caption describes the designations of the MQW structures discussed below. The observation of sharp and narrow satellite peaks [up to the sixth order in structure A, Fig. 3(a)] confirms the formation of the abrupt interfaces and realization of a quite uniform period in the MQW structures grown at the Me-rich conditions. The simulation of the diffraction patterns using the commercial software package PANalytical X'pert Epitaxy confirmed the intended GaN and AlN thicknesses with an accuracy of ±0.5 ML. It should be noted that the good matching between the positions of all of the experimental and simulation peaks implies the coherent growth of the GaN/AlN MQW structures on the AlN buffers. Therefore, one can assume generation of a rather high compressive stress during the growth of the structures with large numbers of QWs. However, a measurement of the substrate curvature by MOSS revealed different behaviors of the average stresses in the GaN/AlN MQW structures with different d_w.

Figure 3(e) shows the temporal variation of the substrate curvature in structure B. The curvature exhibits short-period oscillations with a more positive (tensile) incremental stress during the AlN growth at the slightly Al-rich conditions, whereas the curvature (stress) decreases when the structure is exposed to the active nitrogen flux. These variations can be explained by introduction of an additional surface stress during Al-rich phases of AlN MME when a liquid metal adlayer is formed on the layer surface, as observed, e.g., by Floro et al.[29] for MBE of GeSi layers. The growth of the GaN QW under the Ga-rich conditions, followed by the Al-rich barrier growth, starts the new period, as shown in the inset in Fig. 3(f). Despite this short-period stress variation, the average stress in this structure remains zero. A different character of the stress evolution is observed in the GaN/AlN MQW heterostructures with $d_w = 1$ nm (~4 MLs) (or more). Figure 3(f) shows the curvature variation during the growth of a 1.8-μm-thick MQW structure D, where not only the short-period stress variation, but also a gradual transition from the initial compressive average stress to the constant tensile stress is observed.

The unusual stress-free growth of the 1.5 ML-GaN/AlN MQW structures could be explained by the elastic relaxation of the GaN in-plane lattice parameter during the formation of bottom and top interfaces in this structure. Such relaxation proceeds at the bottom interface through development of discontinuities in the GaN layer, leading to formation of ultra-thin spatially separated platelets with thicknesses of few MLs, which was considered by Bourret et al.[30] as an effective stress-relaxation mechanism at the onset of PAMBE growth of GaN-on-AlN structures at Me-rich conditions. This

© 2018 The Japan Society of Applied Physics

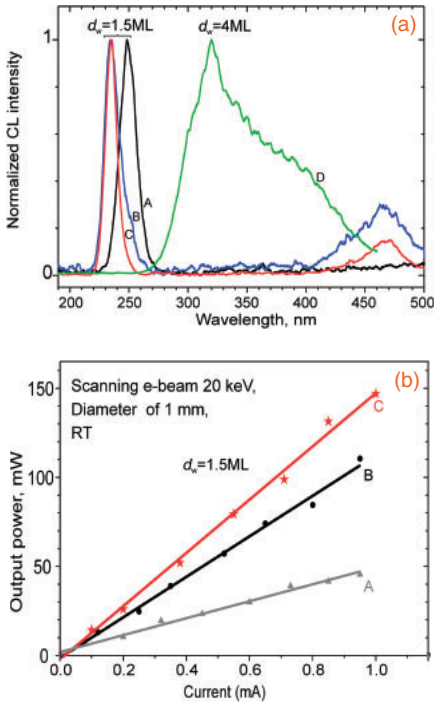

Fig. 4. (a) Normalized RT CL spectra of the GaN/AlN MQW structures A, B, C, and D, measured at $E_e = 10$ keV, $I_e = 0.1$ mA, and beam spot diameter of ~1 mm. (b) Output power as a function of the current of the pulse-scanning e-beam with $E_e = 20$ keV, measured at RT, for the 1.5-ML-GaN/AlN MQW structures A, B, and C.

should obviously lead to a smaller distortion of the GaN vertical lattice parameter than that in a continuous GaN ML. Moreover, the XRD data showing the averaged MQW lattice parameter (0th-order peak) matching precisely to that of the AlN buffer [Figs. 3(a)–3(c)] indicate that the reverse elastic relaxation of the GaN in-plane lattice parameter in platelets toward the AlN parameter occurs at the upper GaN/AlN interface, which also causes a small distortion of the in-plane lattice parameter of the first AlN capping MLs. Therefore, the GaN/AlN MQW structures with extremely thin GaN QWs (1–2 MLs) can demonstrate a coherent and stress-free growth on AlN with a constant average substrate curvature. These GaN quantum platelets can probably serve as efficient carrier localization sites in the QW plane, as discussed above in the PL section (Fig. 2).

However, for the MQW structures with thicker GaN QWs (≥4 MLs) and average Al content of $x_{av} = 0.93$ (structure D), the mechanism of the reversible elastic relaxation through formation of separate platelets is apparently broken. This leads to the non-monotonous behavior of the average stress with a sign change at ~0.6 μm, which is similar to that of thick Al-rich AlGaN alloy layers grown coherently on AlN at low temperatures, inherent for PAMBE.[31] Consequently, we observe a noticeable lattice mismatch between the MQW 0th-order XRD peak and AlN buffer peak [Fig. 3(d)], as well as strain-induced asymmetric broadening of the MQW higher-order satellites.

The possibility of stress-free growth of thick GaN/AlN MQW structures with a number of QWs up to 360 was employed for fabrication of EBP sub-240-nm UV emitters. In these structures, the 2-μm-thick MQW active region can be efficiently excited as a whole by the e-beam with an energy of $E_e \sim 20$ keV. The sufficiently small barrier width (5–6 nm) ensures fast collection of non-equilibrium carriers into the QWs. Figure 4(a) shows CL spectra for the MQW structures A, B, C, and D, excited by an e-beam with $E_e = 10$ keV. The observation of single peaks for the structures A, B, and C with a spectral width of ~20 nm and peak position varied in the narrow range of 235–250 nm implies a sufficiently good reproducibility of the MQW structure parameters during long-term growth cycles. In contrast, structure D with the thicker wells (4 MLs) exhibits a large red-shift of the CL peak energy due to the reduced quantum confinement and enhanced QCSE. In addition, it exhibits a significant broadening of the CL peak, which can be explained by the complex evolution of the stress in the structure [see Fig. 3(f)], affecting the radiative characteristics of the QWs due to the variable internal polarization fields.

Figure 4(b) shows the UV-light output powers of the structures A, B, and C ($d_w \sim 1.5$ ML) as a function of the e-beam pumping current I_e varied up to 1 mA at $E_e = 20$ keV. The e-beam had a diameter of ~1 mm and was scanned along a certain line across the structure surface, covered by a thin Al film, with a scan velocity of 4×10^5 cm/s and repetition rate of 50 Hz. The UV radiation was extracted through a sapphire substrate. Structure C with the maximum number of QWs of 360 exhibited the maximum pulse output power of $P_{out} \sim 150$ mW at 235 nm, corresponding to a wall plug efficiency (WPE) of 0.75%, which by ~70% exceeds the WPE value of 0.44% achieved for EBP emitters based on MOVPE-grown AlGaN MQWs, demonstrating the highest-reported pulse output power of 230 mW at 246 nm.[23] The CW output powers, measured using an e-beam with a diameter of 10 mm at $E_e = 15$ keV and $I_e = 0.45$ mA, were $P_{out} = 7$, 14, and 28 mW for the MQW structures with N of (A) 40, (B) 120, and (C) 360, respectively. The increase in the output power with the number of QWs may be due to better transport and capture of excited charge carriers in the structures with thinner barriers, as well as larger volume of the active region; no special post-growth processing treatment, similar to that used in Ref. 11 to increase the external quantum efficiency of the UV output by a factor of 1.5, was performed in this case.

In summary, a detailed investigation of the PAMBE Me-rich growth and structural properties of the binary GaN/AlN MQW structures with well widths varied in the range of 1–4 MLs confirmed the formation of the abrupt symmetric QW interfaces and good reproducibility of the QW parameters through the multi-period structures (up to 360), and revealed the stress-free coherent growth of the $\{GaN/AlN\}_{360}$ MQW structures with the thinnest (1.5 ML) QWs on 1.5-μm-AlN/c-Al_2O_3 PAMBE templates. The latter effect was explained by the lateral elastic strain relaxation within the 1.5-ML-thick QWs through formation of few-ML-thick GaN platelets, which led to an efficient non-equilibrium carrier confinement and significant increase in the IQE. The high-power e-beam-pumped deep-UV emitters with a wavelength of ~235 nm were fabricated based on the $\{1.5\text{-ML-GaN/AlN}\}_{360}$ MQW heterostructures. They exhibited an RT output pulse power as high as 150 mW at the highest reported WPE of ~0.75%.

Acknowledgments This study was partly supported by RSF (No. 14-22-00107) (MBE growth and characterization) and RFBR-BRICS (No. 17-52-80089) (CL studies).

© 2018 The Japan Society of Applied Physics

1) M. Kneissl, in *III-Nitride Ultraviolet Emitters: Technology and Applications*, ed. M. Kneissl and J. Rass (Springer, Cham, 2016) Springer Series in Material Science, Vol. 227, Chap. 1.
2) D. Welch, M. Buonanno, V. Grilj, I. Shuryak, C. Crickmore, A. W. Bigelow, G. Randers-Pehrson, G. W. Johnson, and D. J. Brenner, Sci. Rep. **8**, 2752 (2018).
3) H. M. Ng, R. Harel, S. N. G. Chu, and A. Y. Cho, J. Electron. Mater. **30**, 134 (2001).
4) K. B. Nam, J. Li, M. L. Nakarmi, J. Y. Lin, and H. X. Jiang, Appl. Phys. Lett. **84**, 5264 (2004).
5) K. Kamiya, Y. Ebihara, M. Kasu, and K. Shiraishi, Jpn. J. Appl. Phys. **51**, 02BJ11 (2012).
6) C. Adelmann, J. Brault, J.-L. Rouvière, H. Mariette, G. Mula, and B. Daudin, J. Appl. Phys. **91**, 5498 (2002).
7) V. N. Jmerik, A. M. Mizerov, A. A. Sitnikova, P. S. Kop'ev, S. V. Ivanov, E. V. Lutsenko, N. P. Tarasuk, N. V. Rzheutskii, and G. P. Yablonskii, Appl. Phys. Lett. **96**, 141112 (2010).
8) J. Verma, S. M. Islam, V. Protasenko, P. K. Kandaswamy, H. (Grace) Xing, and D. Jena, Appl. Phys. Lett. **104**, 021105 (2014).
9) V. N. Jmerik, T. V. Shubina, A. M. Mizerov, K. G. Belyaev, A. V. Sakharov, M. V. Zamoryanskaya, A. A. Sitnikova, V. Yu. Davydov, P. S. Kop'ev, E. V. Lutsenko, N. V. Rzheutskii, A. V. Danilchik, G. P. Yablonskii, and S. V. Ivanov, J. Cryst. Growth **311**, 2080 (2009).
10) S. V. Ivanov, D. V. Nechaev, A. A. Sitnikova, V. V. Ratnikov, M. A. Yagovkina, N. V. Rzheutskii, E. V. Lutsenko, and V. N. Jmerik, Semicond. Sci. Technol. **29**, 084008 (2014).
11) X. Rong, X. Wang, S. V. Ivanov, X. Jiang, G. Chen, P. Wang, W. Wang, C. He, T. Wang, T. Schulz, M. Albrecht, V. N. Jmerik, A. A. Toropov, V. V. Ratnikov, V. I. Kozlovsky, V. P. Martovitsky, P. Jin, F. Xu, X. Yang, Z. Qin, W. Ge, J. Shi, and B. Shen, Adv. Mater. **28**, 7978 (2016).
12) Y. Taniyasu and M. Kasu, Appl. Phys. Lett. **99**, 251112 (2011).
13) S. M. Islam, V. Protasenko, S. Rouvimov, H. (Grace) Xing, and D. Jena, Jpn. J. Appl. Phys. **55**, 05FF06 (2016).
14) S. M. Islam, V. Protasenko, K. Lee, S. Rouvimov, J. Verma, H. (Grace) Xing, and D. Jena, Appl. Phys. Lett. **111**, 091104 (2017).
15) C. Liu, Y. K. Ooi, S. M. Islam, H. (Grace) Xing, D. Jena, and J. Zhang, Appl. Phys. Lett. **112**, 011101 (2018).
16) J. K. Kim, E. L. Waldron, Y.-L. Li, Th. Gessmann, E. F. Schubert, H. W. Jang, and J.-L. Lee, Appl. Phys. Lett. **84**, 3310 (2004).
17) S. Inoue, N. Tamari, and M. Taniguchi, Appl. Phys. Lett. **110**, 141106 (2017).
18) D. Liu, S. J. Cho, J. Park, J. Gong, J. H. Seo, R. Dalmau, D. Zhao, K. Kim, M. Kim, A. R. K. Kalapala, J. D. Albrecht, W. Zhou, B. Moody, and Z. Ma, Appl. Phys. Lett. **113**, 011111 (2018).
19) T. Oto, R. G. Banal, K. Kataoka, M. Funato, and Y. Kawakami, Nat. Photonics **4**, 767 (2010).
20) Y. Shimahara, H. Miyake, K. Hiramatsu, F. Fukuyo, T. Okada, H. Takaoka, and H. Yoshida, Appl. Phys. Express **4**, 042103 (2011).
21) F. Fukuyo, S. Ochiai, H. Miyake, K. Hiramatsu, H. Yoshida, and Y. Kobayashi, Jpn. J. Appl. Phys. **52**, 01AF03 (2013).
22) S. V. Ivanov, V. N. Jmerik, D. V. Nechaev, V. I. Kozlovsky, and M. D. Tiberi, Phys. Status Solidi A **212**, 1011 (2015).
23) F. Tabataba-Vakili, T. Wunderer, M. Kneissl, Z. Yang, M. Teepe, M. Batres, M. Feneberg, B. Vancil, and N. M. Johnson, Appl. Phys. Lett. **109**, 181105 (2016).
24) D. V. Nechaev, P. A. Aseev, V. N. Jmerik, P. N. Brunkov, Y. V. Kuznetsova, A. A. Sitnikova, V. V. Ratnikov, and S. V. Ivanov, J. Cryst. Growth **378**, 319 (2013).
25) V. N. Jmerik, A. M. Mizerov, D. V. Nechaev, P. A. Aseev, A. A. Sitnikova, S. I. Troshkov, P. S. Kop'ev, and S. V. Ivanov, J. Cryst. Growth **354**, 188 (2012).
26) P. Bogusławski, K. Rapcewicz, and J. J. Bernholc, Phys. Rev. B **61**, 10820 (2000).
27) N. Gogneau, D. Jalabert, E. Monroy, E. Sarigiannidou, J. L. Rouvière, T. Shibata, M. Tanaka, J. M. Gerard, and B. Daudin, J. Appl. Phys. **96**, 1104 (2004).
28) Z. Gačević, A. Das, J. Teubert, Y. Kotsar, P. K. Kandaswamy, Th. Kehagias, T. Koukoula, Ph. Komninou, and E. Monroy, J. Appl. Phys. **109**, 103501 (2011).
29) J. A. Floro, E. Chason, S. R. Lee, R. D. Twesten, R. Q. Hwang, and L. B. Freund, J. Electron. Mater. **26**, 969 (1997).
30) A. Bourret, C. Adelmann, B. Daudin, J.-L. Rouvière, G. Feuillet, and G. Mula, Phys. Rev. B **63**, 245307 (2001).
31) O. A. Koshelev, D. V. Nechaev, S. I. Troshkov, V. V. Ratnikov, V. N. Jmerik, and S. V. Ivanov, J. Phys.: Conf. Ser. **1038**, 012061 (2018).

© 2018 The Japan Society of Applied Physics